Changing links between South Asian summer monsoon circulation and tropospheric land-sea thermal contrasts under a warming scenario

Ying Sun,[1] Yihui Ding,[1] and Aiguo Dai[2]

Received 4 November 2009; revised 2 December 2009; accepted 15 December 2009; published 21 January 2010.

[1] Forced with increased greenhouse gases, the South Asian summer monsoon (SASM) circulation weakens in climate models, which appears inconsistent with the projected increases in near-surface land-sea thermal contrasts during the 21st century. Our analysis shows that the SASM intensity positively correlates with the land-sea thermal contrast in both the lower- and upper-troposphere before year 2000; thereafter a reduced upper-tropospheric thermal contrast leads to a weakened SASM circulation, despite an increasing lower-tropospheric thermal contrast. The decrease in the upper-tropospheric thermal contrast mainly results from enhanced upper-tropospheric warming over the tropical Indian Ocean due to increased latent heating. The results suggest a crucial role of enhanced tropical convection in the weakening of SASM circulation and a weak influence of lower-tropospheric thermal contrast on the SASM under global warming. They also imply a less important role of near-surface processes over the Tibetan Plateau in the long-term SASM change during the 21st century. **Citation:** Sun, Y., Y. Ding, and A. Dai (2010), Changing links between South Asian summer monsoon circulation and tropospheric land-sea thermal contrasts under a warming scenario, *Geophys. Res. Lett.*, *37*, L02704, doi:10.1029/2009GL041662.

1. Introduction

[2] The response of the South Asian summer monsoon (SASM) to increased atmospheric CO_2 and other greenhouse gases (GHGs) has received considerable attention [e.g., *Kripalani et al.*, 2007a; *Meehl et al.*, 2007a]. As GHGs increase, most models suggest larger surface warming over the Asian continent than over the tropical oceans, with the near-surface land-sea thermal contrast becoming larger in summer [*Meehl et al.*, 2007a]. Since the SASM is traditionally thought to be driven by the land-sea thermal contrast between the Asian continent and its adjacent oceans to the south [*Fu and Fletcher*, 1985; *Li and Yanai*, 1996], the increased land-sea thermal contrast would imply an enhanced SASM circulation. Although a few early studies reported enhanced [*Zhao and Kellogg*, 1988] or little changed [*Ashrit et al.*, 2003] SASM circulation in response to increased GHGs in some individual models, most recent coupled global climate models (CGCMs) project a weakened SASM circulation under various scenarios of increased GHGs [*Ueda et al.*, 2006; *Kripalani et al.*, 2007a; *Meehl et al.*, 2007a]. This presents an apparent paradox between the increased near-surface land-sea thermal contrast and weakened SASM circulation in projected future climates. The monsoon over East Asia is, however, projected to strengthen as evidenced by the projected intensification of the North Pacific Subtropical High [*Kripalani et al.*, 2007b].

[3] Previous studies have used different definitions of the land-sea thermal contrast to study SASM variations, such as the land-sea differences of near-surface temperature [*Fu and Fletcher*, 1985], 200–500 hPa thickness [*Li and Yanai*, 1996; *Ueda et al.*, 2006], and 200–1000 hPa thickness [*Holton*, 2004]. These studies have shown that the thermal difference at different levels between the Asian continent, especially the Tibetan Plateau (TP), and the tropical oceans is closely linked to the establishment, seasonal evolution, and interannual to interdecadal variations of the SASM. The dominant controlling factors include the sea surface temperature (SST) in the Pacific (remote) and Indian (local) Oceans and the land-surface processes over Asia. They influence the SASM by changing the land-sea thermal contrast through atmospheric large-scale circulation, sensible and latent heating, and other processes [*Yang and Lau*, 2006]. *Ueda et al.* [2006] suggested that the model-projected weakening of the SASM circulation may result from a reduction in the upper-tropospheric meridional thermal gradient between the Asian continent and the oceans to the south.

[4] These previous studies all show a positive correlation between the SASM intensity and the thermal contrast at different levels in historical records. This relationship appears to have changed in model-projected warmer climates, because a weakened SASM is accompanied by enhanced near-surface thermal contrast. However, it is unclear why this could happen in the models. This suggests that the SASM's relationship with the land-sea thermal contrast may change with increasing GHGs. This study aims to address these issues and investigate what processes control the SASM circulation change under GHGs-induced global warming.

2. Data and Methods

[5] The model data for the period from 1951 to 2099 were extracted from the Intergovernmental Panel on Climate Change (IPCC) simulations for the 20th century (20C3M) and the 21st century under the SRES A1B (a medium) emissions scenario using CGCMs for the Fourth Assessment (AR4) [*Meehl et al.*, 2007b] (also see http://www-pcmdi.llnl.gov/ipcc/about_ipcc.php). Here monthly data from seven

[1]National Climate Center, China Meteorological Administration, Beijing, China.
[2]National Center for Atmospheric Research, Boulder, Colorado, USA.

0094-8276/10/2009GL041662$05.00

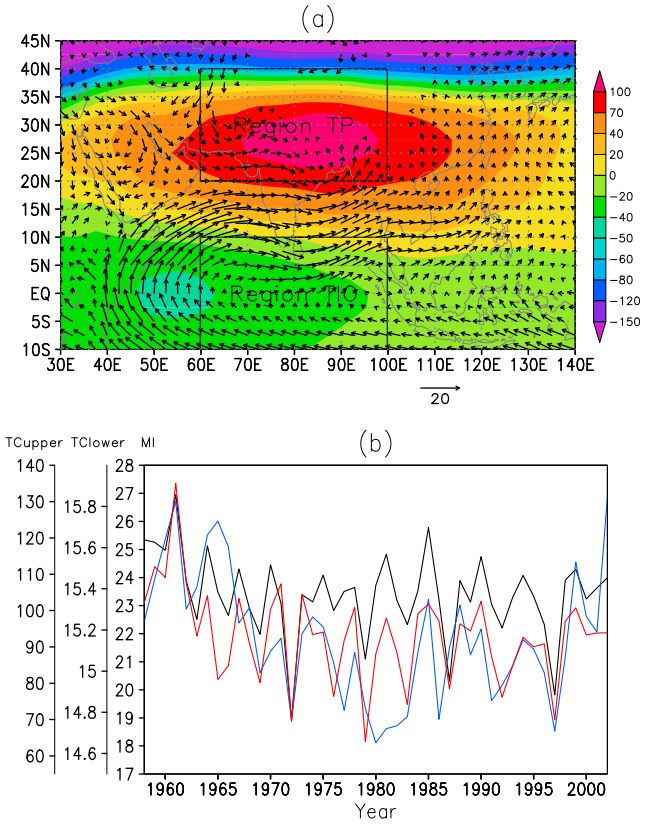

Figure 1. (a) Long-term (1979–2000) mean of June-July-August-September (JJAS) 850 hPa winds (arrows, in m s^{-1}) and 200–500 hPa thickness anomaly (colors, in geopotential meter [gpm]) relative to the mean of the domain (10°S–45°N, 30°–140°E). (b) Temporal evolution of the JJAS *MI* (black, m s^{-1}), TC_{upper} (red, gpm), and TC_{lower} (blue, gpm) from 1958 to 2002 in the ERA-40 reanalysis. See text for the details.

models were used after evaluating 19 AR4 models' performance in simulating the SASM circulation. These seven models reasonably reproduce the SASM circulation intensity and its relationship with the tropospheric land-sea thermal contrasts during the later half of the 20th century. They include: CGCM3.1(T63), GFDL-CM2.1, INM-CM3.0, ECHAM5/MPI-OM, MRI-CGCM2.3.2, PCM, and UKMO_HadGEM1. We also used the ERA-40 reanalysis monthly data for 1958–2002 [*Uppala et al.*, 2005]. All the data were linearly interpolated onto a 2.5° × 2.5° grid.

[6] The SASM index (*MI*) defined by Webster and Yang [1992] was chosen as a proxy for changes in the SASM circulation intensity (SASM intensity hereafter). This *MI* is defined as the difference of zonal winds at 850 (U_{850}) and 200 hPa (U_{200}) levels (i.e., $MI = U_{850} - U_{200}$) averaged over 0°–20°N and 40°–110°E. This dynamical index depicts the thermally-driven nature of the SASM and thus recognizes the importance of horizontal thermal difference. The land-sea thermal contrast for June-July-August-September (JJAS) between the TP region (20°–40°N, 60°–100°E) and the tropical Indian Ocean (TIO, 10°S–10°N, 60°–100°E) (see the black boxes in Figure 1a) was computed for both the upper and lower troposphere using TC_{upper} = *Thickness* (*200–500 hPa, TP*) − *Thickness* (*200–500 hPa, TIO*) and TC_{lower} = *Temperature* (*near-surface* [*2m*], *TP*) − *Temperature* (*500–850 hPa, TIO*). The 500–850 hPa temperature over the TIO is used as a proxy of near-surface temperature after height adjustment for comparison with 2 m air temperature over the TP, which is 2–5 km above the mean sea level. For convenience, the near-surface (i.e., 2 m) air temperature over the TP and 500–850 hPa temperature over the TIO are referred to as lower-tropospheric temperature and the 200–500 hPa thickness is referred to as upper-tropospheric thickness hereafter. Since the focus of this paper is on the SASM circulation change, SASM hereafter refers to SASM circulation unless stated otherwise.

3. Changes in the *MI*, TC_{upper} and TC_{lower}

[7] Figure 1a shows the 1979–2000 mean JJAS 850 hPa winds (arrows), and 200–500 hPa thickness anomalies (colors; relative to the mean of the domain: 10°S–45°N, 30°–140°E) from the ERA-40 reanalysis. The thickness anomalies centered over the TP and the TIO form a large meridional thermal gradient between Asia and the TIO, which drives the low-level southwesterly winds from the northern Indian Ocean through the Bay of Bengal to the South China Sea (Figure 1a) and high-level northeasterly winds from Asia to the Southern Hemisphere (not shown). The maintenance, internannual, and interdecadal variations of the SASM circulation is closely linked this meridional land-sea thermal gradient, which has been defined differently either using temperature or layer-thickness differences in lower or upper troposphere [e.g., *Fu and Fletcher*, 1985; *Li and Yanai*, 1996]. Figure 1b clearly shows the close links between the TP-TIO thermal contrast and the SASM intensity. All three series show a rapid decrease from 1960 to 1980 and thereafter a slight increase. The temporal variations are significantly correlated among the JJAS *MI* (black), TC_{upper}(red), and TC_{lower} (blue), with the correlation coefficient $r = 0.84$ between *MI* and TC_{upper}, and 0.51 between *MI* and TC_{lower} during 1958–2002 in the ERA-40. These positive correlations suggest that a strong (weak) monsoon is accompanied by large (small) lower- and upper-tropospheric TP-TIO thermal contrasts in the ERA-40 reanalysis. Another important feature is that over both the TP and TIO, there exists significant correlation ($r = 0.59$ for the TP and 0.59 for the TIO) between the lower-layer temperature and upper-layer thickness, which leads to significant correlation ($r = 0.54$) between the TC_{lower} and TC_{upper} shown in Figure 1b. This consistent evolution indicates tight coupling between the upper- and lower-layer thermal variables over the SASM regions. It explains why the SASM variations can be related to the land-sea thermal contrast defined at both lower and upper tropospheric levels in previous studies. On the other hand, the correlation between the SASM precipitation (averaged over 5°N–35°N, 60°E–100°E, not shown) and the *MI*, TC_{upper} and TC_{lower} are relatively weak, with $r = 0.38$, 0.51 and 0.27 during 1958–2002, respectively. This indicates that the dynamic *MI* index is not a very good measure of surface rainfall in the whole SASM region. This also applies to the 21st century model results discussed below.

[8] The model-simulated JJAS *MI* (black), TC_{upper}(red), and TC_{lower} (blue) from 1951–2099 are shown in Figure 2a

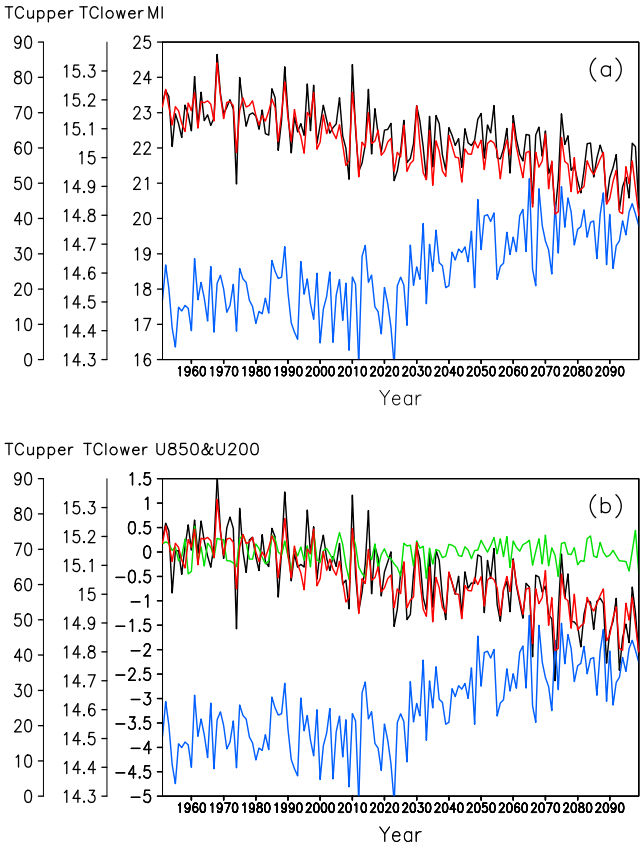

Figure 2. Temporal evolution of (a) JJAS *MI* (black, in m s^{-1}), TC_{upper} (red, gpm), and TC_{lower} (blue, gpm), and (b) JJAS $-U_{200}$ (black, m s^{-1}) and U_{850} (green, m s^{-1}) anomalies (relative to 1980–1999 mean) averaged over 0°–20°N and 40°–110°E, and TC_{upper} (red, gpm), and TC_{lower} (blue, gpm) from 1951 to 2099 based on IPCC AR4 7-model arithmetic mean under observation-based forcing during 1951–2000 and the A1B scenario for 2001–2099. U_{200} anomalies in Figure 2b were multiplied by −1 to show the weakening of 200 hPa easterly winds.

using the 7-model arithmetic mean. As in the ERA-40, the simulated inter-annual to multi-year variations are correlated among these indices from 1951–2000, with r = 0.80 between *MI* and TC_{upper}, and 0.48 between *MI* and TC_{lower}. The models generally reproduce the positive influence of near-surface temperature on the upper-layer thickness during 1951–2000. However, during the 21st century, the TC_{lower} increases whereas both the *MI* and TC_{upper} decrease, leading to a correlation of 0.88 between *MI* and TC_{upper} and −0.10 (mainly due to opposite trends) between *MI* and TC_{lower} (r = 0.85 and 0.34, respectively, after removing the trends and low-frequency variations). Figure 2b compares the time series of 850 hPa (U_{850}, black) and 200 hPa ($-U_{200}$, green) zonal winds anomalies averaged over 0°–20°N and 40°–110°E with the TC_{upper} (red) and TC_{lower} (blue) indices. It is clear that $-U_{200}$ decreases rapidly since the late 20th century whereas U_{850} stays relatively stable. This indicates that the decreasing trend in MI(= U_{850} − U_{200}) results mainly from the large decreases in 200 hPa easterly winds. The rapid decrease in $-U_{200}$ is accompanied by the decreasing TC_{upper} (r = 0.89 and 0.84 for variations with and without 9-year running mean), suggesting that the weakening of the upper-level zonal winds is related to the decreasing upper-layer thermal contrast (i.e., $TC_{upper,}$) in the 21st century. On the other hand, the correlation between the TC_{lower} and U_{850} changes from r = 0.47 from 1951–2000 to r = 0.25 during the 21st century, indicating a weakened relationship between TC_{lower} and U_{850}.

[9] These results suggest that the lower-tropospheric thermal contrast is no longer a good indicator of the SASM intensity in the 21st century, although the two still correlate on multi-year time scales (r = 0.34). Also note the correlation between TC_{upper} and TC_{lower} changes from r = 0.32 for 1951–2000 to r = −0.27 for 2001–2099 (r = 0.31 and 0.25 after long-term trends removed), indicating a weakened coupling between TC_{lower} and TC_{upper} and thus a smaller influence of lower-layer thermal conditions on the SASM in a warmer climate.

[10] In the models, the linear trends of upper-layer thickness from 2001–2099 are 12.24 geopotential meter (gpm)/10yr over the TP and 13.73 gpm/10yr over the TIO, whereas the trend of lower-tropospheric temperature is 0.36 K/10yr over the TP and 0.32 K/10yr over the TIO, respectively. Thus, it is the slower warming in the upper troposphere over the TP than over the TIO that leads to the decrease of TC_{upper}, whereas it is the larger increase of lower-layer temperature over the TP than over the TIO that results in the increase of TC_{lowerr}. The models also underestimate mean *MI* and the two thermal contrasts considerably during 1951–2000 compared with the ERA-40 reanalysis (Figure 1b and 2), which suggests that the land-sea thermal contrasts and the associated SASM circulation are too weak in the model mean climate. Further analysis revealed that this is mainly caused by the smaller 200–500 hPa thickness over the TP in the models, which may reflect the models' deficiency in resolving the complex terrain over the TP.

[11] To help understand the above changes, Figure 3a shows tropospheric temperature changes as a function of height averaged over the TIO region from 1951–2099. The vertical structure of the temperature anomalies changes around year 2000 from a vertically-uniform pattern to more rapid warming in the upper troposphere, which indicates reduced influence of near-surface temperature on the upper-layer thermal condition in the 21st century. A similar change is also found over the TP (not shown), but with less enhanced warming in the upper troposphere in the 21st century. Thus, in a GHG-induced warmer climate, the enhanced upper-tropospheric warming over the TIO outpaces the warming over the TP, which is consistent with the maximum warming around 200 hPa over the tropics (Figure 3b) that primarily results from enhanced latent heating from increased tropical precipitation [*Dai et al.*, 2001]. As a result of the differential warming, there is a maximum decrease in the meridional temperature gradient (temperature changes averaged from 20°–40°N minus that from 10°S–10°N) around 500–150 hPa in the longitudinal belt of 40°–100°E, along with the increased gradients at the lower troposphere there (Figure 3c). From 1951–1999, the 200–500 hPa thickness over the TP and TIO increase at similar rates (Figure 3d). However, in the 21st century the increase of 200–500 hPa thickness over the TIO becomes much faster than that over the TP, resulting in a difference of

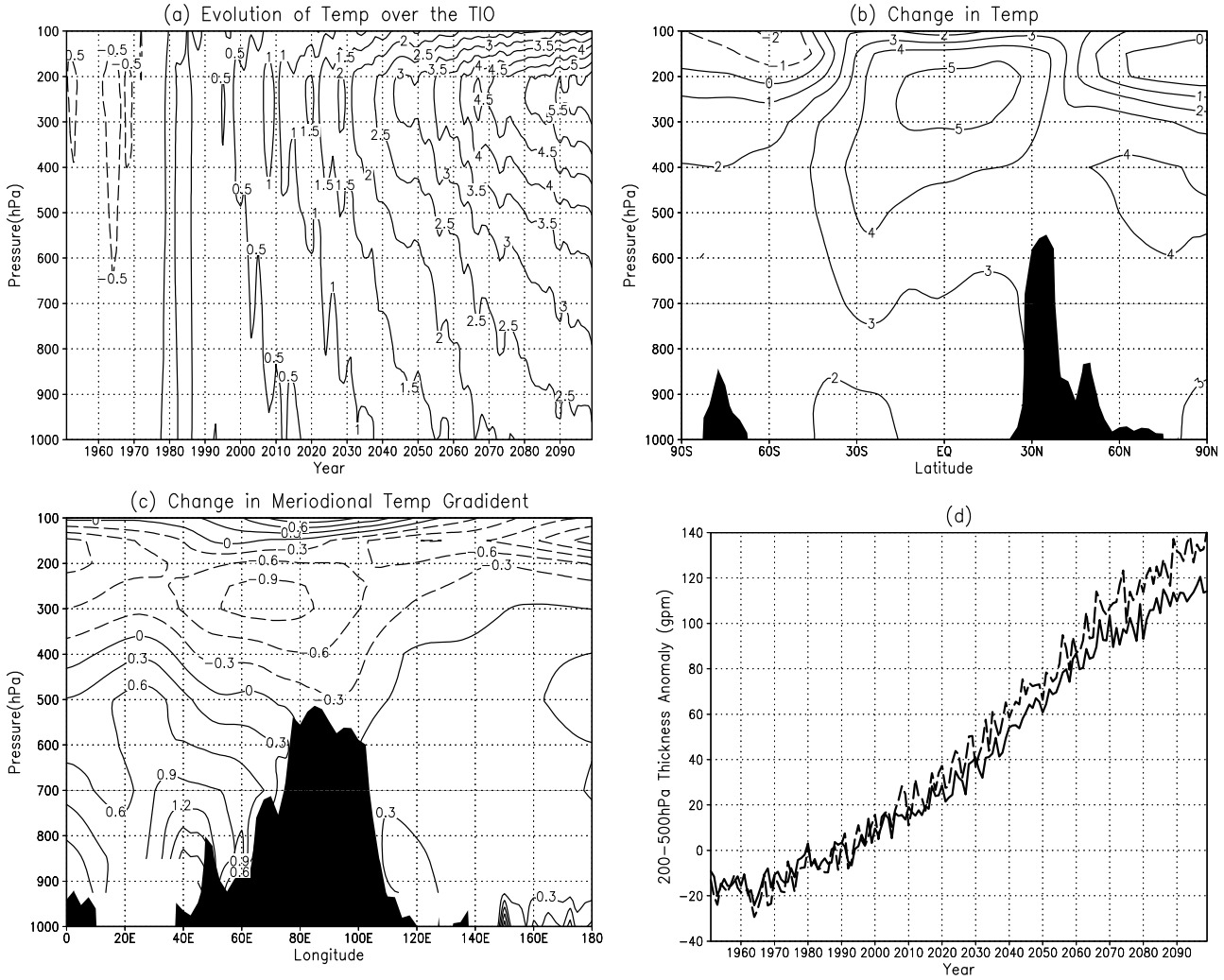

Figure 3. IPCC 7-model averaged (a) time-height cross-section of JJAS temperature departures (K, from 1980–1999 mean) averaged over the TIO during 1951–2099. (b) Latitude-height cross-section of JJAS temperature change (K) from 1980–1999 to 2080–2099 averaged between 60°E and 100°E. The topography along 90°E is shown by the black areas. (c) Longitude-height cross-section of change (K, from 1980–1999 mean) in JJAS meridional temperature gradient (temperature changes averaged from 20°–40°N minus that from 10°S–10°N) for 2080–2099. The topography along 35°N is shown by the black areas. (d) Time series of JJAS 200–500 hPa thickness anomalies (gpm, from 1980–1999 mean) over the TP (solid line) and TIO (dashed line) during 1951–2099.

~30gpm by 2099 (Figure 3d). Further analysis revealed that the reduced TP-TIO upper-tropospheric thermal contrast is a common feature among the individual models (not shown), which indicates the robustness of the weakening of the SASM circulation in GHG-induced warmer climates.

[12] The above analyses show that the differential increases of the upper-tropospheric temperature over the TIO and TP lead to the changed relationship between the SASM intensity and tropospheric thermal contrasts over the SASM regions in a GHG-induced warmer climate. The weakening of the SASM circulation is directly related to the decrease of upper-tropospheric TP-TIO thermal contrast, which in turn is caused by the larger upper-tropospheric warming over the TIO than over the TP. The fact that the SASM weakens as the lower-tropospheric thermal contrast increases in the 21st century implies a smaller role of this thermal contrast in determining the SASM intensity than suggested by previous studies for the 20th century.

[13] The enhanced upper-tropospheric warming in the Tropics and midlatitudes is a typical feature in global climate models forced by increased GHGs [*Dai et al.*, 2001; *Santer et al.*, 2005]. As the climate warms, atmospheric water vapor content increases exponentially with temperature following the Clausius-Clapeyron equation. In the Tropics, the increased water vapor leads to enhanced latent heating during convection and thus larger warming in the middle-upper troposphere than in the lower levels [*Xu and Emanuel*, 1989]. The enhanced tropical convection also leads to increased high clouds over the low and middle latitudes, which absorb more longwave radiation from the warmer surface and lower layers and thus further enhance the upper-tropospheric warming [*Dai et al.*, 2001]. We found that over the TP areas, most AR4 models also show

an amplification (~1.42 times) of surface warming in the upper troposphere. This enhanced upper-level warming outside the Tropics results from advection of warmer air from the Tropics and enhanced longwave radiative heating due to increased water vapor and clouds at these levels [*Dai et al.*, 2001].

4. Summary and Concluding Remarks

[14] We have analyzed 20th and 21st century simulations by seven selected models participated in the IPCC AR4 under the SRES A1B emissions scenario to investigate the relationship between the SASM circulation intensity and the land-sea thermal contrast in the troposphere over the SASM regions. The results show that for 1951–2000, the SASM intensity (*MI*) is significantly correlated with the TP-TIO thermal contrast in both the lower and upper troposphere (r = 0.48 and 0.80, respectively). In the 21st century, however, the upper tropospheric thermal contrast decreases due to enhanced warming in the tropical upper troposphere, while the lower tropospheric thermal gradient increases because of larger near-surface warming over the TP. The decreasing upper-tropospheric thermal contrast leads to a rapid decline in 200 hPa easterly winds over the SASM region, which in turn results in a decreasing trend in the SASM intensity (*MI*), despite the increasing lower-tropospheric thermal contrast. The downward trend in TC_{upper} dominates over the influence of the increasing trend in TC_{lower} on the SASM circulation change on decadal to longer time scale because of the strong dependence of *MI* on TC_{upper}. On multi-year time scales, both TC_{upper} and TC_{lower} are still positively correlated with *MI* in the 21st century.

[15] Atmospheric latent heating plays an important role in enhancing the land-sea thermal contrast and thus the SASM circulation. Without the latent heating, the SASM circulation would be much weaker than observed [*Webster*, 1987]. However, in a GHG-induced warmer climate, large latent heating over the Tropics increases 200–500 hPa thickness more over the TIO than over the TP. This reduces the land-sea pressure gradient and thus weakens the monsoon circulation intensity.

[16] This study suggests that the enhanced upper-tropospheric warming over the TIO plays a key role in model-projected SASM circulation change. The influence of near-surface temperature on the upper layer thermal condition may weaken over both the TP and TIO in a warming climate. The lower tropospheric thermal contrast and thus the near-surface temperature change over the TP do not control the SASM circulation intensity as GHGs increase. Thus, one should be cautious in using the near-surface or lower-tropospheric fields, such as the snow cover over the TP, to infer future SASM changes.

[17] Because the enhanced upper-tropospheric warming results primarily from increased latent heating from tropical convection, this study implies a crucial role of increased water vapor in SASM's response to increased GHGs. Furthermore, despite the weakened monsoon winds, summer monsoon precipitation in South Asia still increases in most GCMs because of the increased water vapor content and convergence over the SASM region [e.g., *Ueda et al.*, 2006]. Therefore, in the selected seven AR4 models both the increased monsoon precipitation and the decreased monsoon winds in South Asia are mainly caused by the increased water vapor and enhanced tropical convection in a GHG-induced warmer climate.

[18] **Acknowledgments.** We thank the international modeling groups and ECMWF for providing the data used here. This study was supported by Chinese NSFC grant 40605020, the State Key Project in the 11th Five-Year Plan 2007BAC03A01 and 973 Program 2006CB403604. We also thank the two reviewers for their helpful comments. The National Center for Atmospheric Research (NCAR) is sponsored by the U.S. National Science Foundation.

References

Ashrit, R. G., H. Douville, and K. Rupa Kumar (2003), Response of the Indian monsoon and ENSO-monsoon teleconnection to enhanced greenhouse effect in the CNRM coupled model, *J. Meteorol. Soc. Jpn.*, *81*, 779–803, doi:10.2151/jmsj.81.779.

Dai, A., T. M. L. Wigley, B. A. Bovilie, J. T. Kiehl, and L. E. Buja (2001), Climates of the twentieth and twenty-first centuries simulated by the NCAR climate system model, *J. Clim.*, *14*, 485–518, doi:10.1175/1520-0442(2001)014<0485:COTTAT>2.0.CO;2.

Fu, C. B., and J. O. Fletcher (1985), The relationship between Tibet-tropical ocean thermal contrast and interannual variability of Indian monsoon rainfall, *J. Clim. Appl. Meteorol.*, *24*, 841–847, doi:10.1175/1520-0450(1985)024<0841:TRBTTO>2.0.CO;2.

Holton, J. R. (2004), An Introduction to Dynamic Meteorology, *Int. Geophys. Ser*, vol. 88, 4th ed., pp. 380–382, Elsevier Acad., Burlington, Mass.

Kripalani, R. H., J. H. Oh, A. Kulkarni, S. Sabade, and H. S. Chaudhari (2007a), South Asian summer monsoon precipitation variability: Coupled climate model simulations and projections under IPCC AR4, *Theor. Appl. Climatol.*, *90*, 133–159, doi:10.1007/s00704-006-0282-0.

Kripalani, R. H., J. H. Oh, and H. S. Chaudhari (2007b), Response of the East Asian summer monsoon to doubled atmospheric CO_2: Coupled climate model simulations and projections under IPCC AR4, *Theor. Appl. Climatol.*, *87*, 1–28, doi:10.1007/s00704-006-0238-4.

Li, C., and M. Yanai (1996), The onset and interannual variability of the Asian summer monsoon in relation to land-sea thermal contrast, *J. Clim.*, *9*, 358–375, doi:10.1175/1520-0442(1996)009<0358:TOAIVO>2.0.CO;2.

Meehl, G. A., et al. (2007a), Global climate projections, in *Climate Change 2007: The Physical Science Basis. Contribution of Working Group I to the Fourth Assessment Report of the Intergovernmental Panel on Climate Change*, edited by S. Solomon et al., pp. 749–830, Cambridge Univ. Press, Cambridge, U. K.

Meehl, G. A., et al. (2007b), The WCRP CMIP3 multimodel dataset: A new era in climate change research, *Bull. Am. Meteorol. Soc.*, *88*, 1383–1394, doi:10.1175/BAMS-88-9-1383.

Santer, B. D., et al. (2005), Amplification of surface temperature trends and variability in the tropical atmosphere, *Science*, *309*, 1551–1556, doi:10.1126/science.1114867.

Ueda, H., A. Iwai, K. Kuwako, and M. Hori (2006), Impact of anthropogenic forcing on the Asian summer monsoon as simulated by eight GCMs, *Geophys. Res. Lett.*, *33*, L06703, doi:10.1029/2005GL025336.

Uppala, S. M., et al. (2005), The ERA-40 re-analysis, *Q. J. R. Meteorol. Soc.*, *131*, 2961–3012, doi:10.1256/qj.04.176.

Webster, P. J. (1987), The elementary monsoon, in *Monsoons*, edited by J. S. Fein and P. L. Stephens, pp. 5–30, Wiley Intersci., New York.

Webster, P. J., and S. Yang (1992), Monsoon and ENSO: Selectively interactive systems, *Q. J. R. Meteorol. Soc.*, *118*, 877–926, doi:10.1002/qj.49711850705.

Xu, K.-M., and K. A. Emanuel (1989), Is the tropical atmosphere conditionally unstable?, *Mon. Weather Rev.*, *117*, 1471–1479, doi:10.1175/1520-0493(1989)117<1471:ITTACU>2.0.CO;2.

Yang, S., and K.-M. Lau (2006), Interannual variability of the Asian monsoon, in *The Asian Monsoon*, edited by B. Wang, pp. 268–280, Praxis, Chichester, U. K.

Zhao, Z., and W. W. Kellogg (1988), Sensitivity of soil moisture to doubling of carbon dioxide in climate model experiments. Part II: The Asian monsoon region, *J. Clim.*, *1*, 367–378, doi:10.1175/1520-0442(1988)001<0367:SOSMTD>2.0.CO;2.

A. Dai, National Center for Atmospheric Research, PO Box 3000, Boulder, CO 80307, USA.

Y. Ding and Y. Sun, National Climate Center, China Meteorological Administration, 46 Zhongguancun Nandajie, Beijing 100081, China. (sunying@cma.gov.cn)